Helical polymer in cylindrical confining geometries

A. Lamura[1,2], T. W. Burkhardt[2,3], and G. Gompper[2]

[1] *Istituto Applicazioni Calcolo, CNR, Sezione di Bari, via Amendola 122/D, 70126 Bari, Italy*

[2] *Institut für Festkörperforschung, Forschungszentrum Jülich, D-52425 Jülich, Germany*

[3] *Department of Physics, Temple University, Philadelphia, PA 19122, USA*

Abstract

Using an algorithm for simulating equilibrium configurations, we study a fluctuating helical polymer either (i) contained in a cylindrical pore or (ii) wound around a cylindrical rod. We work in the regime where both the contour length and the persistence length of the helical polymer are much larger than the diameter of the cylinder. In case (i) we calculate the free energy of confinement and interpret it in terms of a worm-like chain in a pore with an effective diameter that depends on the parameters of the helix. In case (ii) we consider the possibility that one end of the helical polymer escapes from the rod and wanders away. The average numbers of turns at which the helix escapes or intersects the rod are measured in the simulations, as a function of the pitch p_0. The behavior for large and small p_0 is explained with simple scaling arguments.

PACS numbers: 87.15.Aa, 36.20.Ey, 61.25.Hq, 82.70.-y

I. INTRODUCTION

In this paper we study some of the equilibrium statistical properties of a confined helical or ribbon-like polymer. The cases of (i) a polymer contained in a cylindrical pore and (ii) a polymer wound around a cylindrical rod are considered. Some motivation is provided by the following observations:

Biological polymers differ from synthetic polymers in that they are semi-flexible, with a persistence length much larger than the monomer size, and usually have a helical structure. This is well known for DNA, but F-actin also has a double-helical structure, while microtubuli are helical cylinders. The diameter of these biological polymers is in the range of 1 to 25 nm. Polymeric helical structures are also found in self-assembling systems, consisting of either amphiphiles or peptides. In some cases the diameters and pitch lengths are much larger than for the biopolymers mentioned above.

In amphiphilic systems the formation of helical ribbons has been observed in multicomponent mixtures of a bile salt or some other nonionic surfactant, phosphatidylcholine or a fatty acid, and a steroid analog of cholesterol [1, 2]. The ribbons have typical diameters in the range of 5 to 20 μm, and pitch angles between 10 and 60^o. Other examples are ethanolic/water solutions of diacetylenic phospholipids, in which the formation of hollow tubules of diameter 0.6 μm and typical lengths of 10 to 100 μm has been observed [3, 4, 5, 6]. Helically-coiled phospholipid-bilayer ribbons appear as metastable intermediates in the growth of these tubules.

Other systems, which show spontaneous assembly of ribbons, are aqueous solutions of peptides [7, 8, 9, 10]. Depending on the solution conditions, the same peptide exists in different conformations, such as random coils, α-helices, or β-sheets. At not too low peptide concentrations, the molecules self-assemble into long β-sheet structures which form twisted ribbons (with a straight central axis). The width of these ribbons is about 4 nm, and their length is of the order of 500 nm [9, 10]. These ribbons can aggregate due to face-to-face attraction into twisted fibrils of a thickness of 8-10 nm.

Interestingly, in a self-assembling system of gemini surfactants (two surfactant molecules covalently linked at their charged head group), the degree of twist and the pitch of the micrometer-scale ribbons has been found to be tunable by the introduction of opposite-handed chiral counterions [11].

The confinement of polymers in cylindrical tubes is one of the classical problems in polymer physics. For biological polymers, such a confinement occurs, for example, when viral DNA of a bacteriophage squeezes through the narrow tail during DNA injection. Technological advances in the manipulation of single molecules in micro- and nanofluidic devices [12, 13] has fueled interest in the structure and dynamics of biological polymers in confined geometries [14].

Helical and twisted ribbons can be confined not only by external walls, but also by winding around each other, as in the fibril formation of twisted β-sheet peptides mentioned above. The simple model we consider, consisting of a helical wound around a thin cylinder, is a step in this direction but leaves out some important physical features, such as the face-to-face attraction in the fibrils.

II. FREE ENERGY OF CONFINEMENT

The free energy ΔF of confinement of a fluctuating polymer of contour length ℓ in a cylindrical pore of diameter D is defined by

$$\exp(-\Delta F/k_B T) = \frac{Z(D,\ell)}{Z(\infty,\ell)} = p(\ell) \tag{1}$$

Here $Z(D,\ell)$ and $Z(\infty,\ell)$ are the partition functions of the polymer with one end fixed in the presence and absence of the cylindrical confining geometry, respectively. The quantity ΔF represents the work required to squeeze the polymer reversibly into the cylindrical pore. It may be evaluated in simulations by generating polymer configurations with one fixed end in an infinite volume with the Boltzmann probability, computing the fraction $p(\ell)$ of the configurations of arc length ℓ which lie entirely within a cylindrical domain of diameter D, and making use of Eq. (1)

For a flexible, self-avoiding polymer with vanishing bending rigidity, ΔF is purely entropic. The confinement of such a polymer in a cylindrical pore is considered in Refs. [15, 16, 17].

In the worm-like chain model of a semi-flexible polymer, the polymer is represented by an inextensible line or filament $\mathbf{r}(s)$ with contour length ℓ and elastic energy

$$E_{\rm worm} = \frac{\kappa}{2}\int_0^\ell \left(\frac{d\mathbf{t}_3}{ds}\right)^2 ds\ . \tag{2}$$

Here s specifies distance along the contour, $\mathbf{t}_3 = d\mathbf{r}/ds$ is the unit tangent vector, κ is the bending rigidity, and $P = \kappa/k_BT$ is the the persistence length. In the narrow-pore, long-polymer limit $D \ll P \ll \ell$, the polymer is almost a straight line, i.e. the angle between the tangent vector $\mathbf{t}_3$ and the z axis or symmetry axis of the cylinder is a small quantity. In this case the right-hand side of Eq. (1) decays as

$$p(\ell) \sim e^{-E_0 \ell} \tag{3}$$

for large ℓ, where $\exp(-E_0\, dz)$ is the largest eigenvalue of the transfer matrix of a slice of the system of thickness dz. The quantity E_0^{-1} represents a typical contour length at which the configurations intersect the pore wall. According to Eqs. (1) and (3) the confinement free energy per unit length $\Delta f = \Delta F/\ell$ is given by

$$\frac{\Delta f}{k_BT} = E_0(P, D) = \frac{A_\circ}{P^{1/3} D^{2/3}} \,, \tag{4}$$

where the dependence on P and D follows from simple scaling or dimensional arguments [18, 19, 20]. Similarly, for a pore with a rectangular cross section with edges $L_1, L_2 \ll P$,

$$\frac{\Delta f}{k_BT} = E_0(P, L_1, L_2) = \frac{A_\square}{P^{1/3}} \left(\frac{1}{L_1^{2/3}} + \frac{1}{L_2^{2/3}} \right) \,. \tag{5}$$

The quantities $A_\circ$ and $A_\square$ on the right-hand sides of Eqs. (4) and (5) are dimensionless universal numbers $A_\circ$ and $A_\square$, which are the same for all worm-like chains.

The prediction $A_\square = 1.1036$ was obtained in Ref. [20] by solving an integral equation numerically which arises in an exact analytical approach. Measuring the probability $p(\ell)$ in Eq. (3) in simulations, fitting the large ℓ behavior with the exponential form (3), and making use of Eqs. (4) and (5), Bicout and Burkhardt [21] estimated

$$A_\circ = 2.375 \pm 0.013 \,, \qquad A_\square = 1.108 \pm 0.013 \,. \tag{6}$$

An earlier estimate from simulations, $A_\circ = 2.46 \pm 0.07$, was given by Dijkstra *et al.* [19].

III. HELICAL POLYMER MODEL

In this paper we generalize the above results to helical polymers or chiral ribbons, which have spontaneous curvature and torsion. Again the polymer is replaced by a curve $\mathbf{r}(s)$ of fixed contour length $\mathcal{S}$. To each point on the line a right-handed triad of unit vectors

$\mathbf{t}_1(s), \mathbf{t}_2(s), \mathbf{t}_3(s)$ is assigned, where $\mathbf{t}_3 = d\mathbf{r}/ds$ is the tangent vector and $\mathbf{t}_1$, $\mathbf{t}_2$ correspond to principal axes of the polymer cross section. The rotation of the triad along the curve is governed by the generalized Frenet equations [22, 23, 24]

$$\frac{d\mathbf{t}_i}{ds} = \boldsymbol{\omega} \times \mathbf{t}_i \ , \quad \boldsymbol{\omega} = \mathbf{t}_1\omega_1 + \mathbf{t}_2\omega_2 + \mathbf{t}_3\omega_3 \ , \tag{7}$$

or

$$\frac{d\mathbf{t}_i}{ds} = \sum_{j,k} \epsilon_{ijk}\mathbf{t}_j\omega_k \ . \tag{8}$$

The elastic energy is given by [22, 23, 24]

$$E_{\rm helix} = \frac{1}{2}\sum_{j=1}^{3} b_j \int_0^{\mathcal{S}} ds \left[\omega_j(s) - \omega_{0j}(s)\right]^2 \ , \tag{9}$$

where the coefficient b_1 and b_2 are bending rigidities along the principal axes of the cross section, and b_3 is the twist rigidity. The parameters $\omega_j(s)$ and $\omega_{0j}(s)$ determine the curvatures and torsions in the deformed and stress-free states of the polymer, respectively. Since the energy is quadratic in the deviations $\delta\omega_j = \omega_j - \omega_{0j}$, the distribution of $\delta\omega_j$ is Gaussian, with zero mean and second moment

$$\langle \delta\omega_i(s)\delta\omega_j(s')\rangle = \frac{k_BT}{b_i}\,\delta_{ij}\,\delta(s-s') \ . \tag{10}$$

We restrict our attention to the case $\omega_{0j}(s) =$ constant, corresponding to a helical polymer with spontaneous curvature and torsion but without spontaneous twist. In the absence of fluctuations, i.e. in the limit $b_1 = b_2 = b_3 = \infty$, the Frenet equations are readily solved [25], yielding

$$\begin{aligned}\mathbf{r}(s) = \mathbf{r}(0) \ + \ \frac{1}{\omega_0}\Bigg\{ & \mathbf{t}_3(0)\sin(\omega_0 s) + \mathbf{e}(0)\,\omega_{03}\left[s - \frac{\sin(\omega_0 s)}{\omega_0}\right] \\ & + \ \mathbf{e}(0)\times\mathbf{t}_3(0)\left[1-\cos(\omega_0 s)\right]\Bigg\} \ ,\end{aligned} \tag{11}$$

where

$$\mathbf{e}(s) = \mathbf{t}_1(s)\frac{\omega_{01}}{\omega_0} + \mathbf{t}_2(s)\frac{\omega_{02}}{\omega_0} + \mathbf{t}_3(s)\frac{\omega_{03}}{\omega_0} \ , \quad \omega_0 = \left(\omega_{01}^2 + \omega_{02}^2 + \omega_{03}^2\right)^{1/2} \ . \tag{12}$$

Equation (11) represents a helix with radius r_0 and pitch p_0, where

$$r_0 = \frac{(\omega_{01}^2 + \omega_{02}^2)^{1/2}}{\omega_0^2} \ , \quad p_0 = 2\pi\frac{\omega_{03}}{\omega_0^2} \ , \tag{13}$$

winding around an axis pointing in the direction of the unit vector $\mathbf{e}(0)$.

Including Gaussian fluctuations according to Eq. (10), Panyukov and Rabin [22, 23] showed that

$$\langle \mathbf{t}_i(s) \cdot \mathbf{t}_j(0) \rangle = \left(e^{-\mathbf{\Gamma} s} \right)_{ij} \ , \tag{14}$$

where $\mathbf{\Gamma}$ is the matrix with elements

$$\Gamma_{ij} = \frac{1}{2} k_B T \left(\sum_k b_k^{-1} - b_i^{-1} \right) \delta_{ij} - \sum_k \epsilon_{ijk} \omega_{0k} \ . \tag{15}$$

The two-point correlation function of the unit vector $\mathbf{e}(s)$ in Eq. (12), which is directed along the axis of the helix, follows from this result. In the special case $b = b_1 = b_2 = b_3$ considered in our simulations,

$$\langle \mathbf{e}(s) \cdot \mathbf{e}(0) \rangle = e^{-s/L_p} \ , \quad L_p = \frac{b}{k_B T} \ , \tag{16}$$

where L_p is the persistence length.

IV. SIMULATIONS

Following Kats *et al.* [24], we replace the differential equations (8) by the difference equations

$$t_{ik}(s + ds) = \sum_j O_{ij} t_{jk}(s) \tag{17}$$

in our simulations. Here t_{ik} denotes the k-th component of $\mathbf{t}_i$ with respect to a fixed Cartesian coordinate system, O is the orthogonal matrix

$$O = \left(1 + \frac{1}{2} A \, ds \right) \left(1 - \frac{1}{2} A \, ds \right)^{-1} \ , \tag{18}$$

and A is the antisymmetric matrix with elements $A_{ij} = \sum_k \epsilon_{ijk} \omega_k$. The difference equations are consistent with the Frenet equations (8) to first order in ds, and the orthogonality of the matrix O preserves the orthonormality of the $\mathbf{t}_i$ in the simulations.

For simplicity we set $b = b_1 = b_2 = b_3$, corresponding to Eq. (16). In accordance with Eq. (10), the $\delta\omega_j(s)$ are chosen randomly from a Gaussian distribution with zero mean and standard deviation $(k_B T / b \, ds)^{1/2}$, where $ds \ll L_p = b/k_B T$.

V. HELICAL POLYMER IN A CYLINDRICAL PORE

We have determined the confinement free energy of a helical polymer fluctuating in a narrow cylindrical pore from simulations. Cylinders with both circular and square cross sections were considered, and we use the same symbol D for the diameter and edge, respectively. The symmetry axis of the cylinder defines the z axis of our fixed coordinate system.

The helical polymer was generated step by step using the numerical procedure described in the preceding Section. The radius r_0 and pitch p_0 were set to desired values by choosing ω_{01}, ω_{03} in Eq. (13) appropriately, with $\omega_{02} = 0$. The starting point was chosen randomly, apart from the requirements that the stress-free helix fit inside the cylinder, with its axis parallel to the z axis. This is the case for the initial vectors $\mathbf{t}_1(0) = (\omega_{03}/\omega_0, 0, \omega_{01}/\omega_0)$, $\mathbf{t}_2(0) = (0, 1, 0)$, and $\mathbf{t}_3(0) = (-\omega_{01}/\omega_0, 0, \omega_{03}/\omega_0)$, which were used. The other simulation parameters were $ds = 10^{-4}$, $D = 1$, $L_p = b_1/k_BT = b_2/k_BT = b_3/k_BT = 8000$. Clearly $ds \ll D \ll L_p$. The pore is narrow in comparison with the persistence length, and ds is small in order to approximate the continuum model (7).

To obtain the free energy of confinement of the helical polymer, we proceeded as discussed below Eq. (1), generating many polymer configurations and computing the probability $P(n)$ that the polymer has not yet intersected the pore wall [26] after n steps of the algorithm. The determination of $P(n)$ was based on $50,000$ independent helices. For large n an exponential decay

$$P(n) \sim e^{-\lambda_0 n} \,, \tag{19}$$

similar to the result (3) for semi-flexible polymers, is expected. According to Eq. (1), the free energy of confinement per unit length along the axis of the helix is given by

$$\frac{\Delta f}{k_BT} = \frac{\lambda_0}{\xi ds} \,, \quad \xi = \frac{p_0}{[p_0^2 + (2\pi r_0)^2]^{1/2}} \,. \tag{20}$$

Here we use the relation $\ell = \xi s$ between the contour length s and the corresponding length ℓ along the axis of the helix. The persistence length L_p, defined with respect to the contour length as in Eq. (16), and the corresponding persistence length P, defined with respect to length along the axis of the helix, also satisfy $P = \xi L_p$.

A helical polymer with persistence length L_p in a pore with diameter $D \ll L_p$ has the same confinement free energy as a semi-flexible polymer with persistence length $P = \xi L_p$ in a pore with effective diameter D_{eff}. To define D_{eff} quantitatively, we equate the free energies

of confinement (4) and (20), obtaining

$$\frac{A_\circ}{D_{\rm eff}^{2/3}} = \frac{(\xi L_p)^{1/3}}{\xi ds}\lambda_0 \ , \quad \frac{A_\square}{D_{\rm eff}^{2/3}} = \frac{(\xi L_p)^{1/3}}{2\xi ds}\lambda_0 \ . \tag{21}$$

The probability $P(n)$ for $r_0 = p_0 = 0.3$, with the other simulation parameters noted above, is shown in Fig. 1. The data are in good agreement with the exponential decay (19), and the values of λ_0 are given in the figure caption. As in the case of a semi-flexible polymer [21], the curves $P(n)$ for the circular and square cylinders practically coincide when plotted versus $\lambda_0 n$ instead of n.

For the exponential decay (19), the mean number of steps of the algorithm at which the polymer intersects the wall equals λ_0^{-1}, corresponding to $N_i = \xi ds/(p_0\lambda_0)$ turns of the helix. The values of λ_0 in the caption of Fig. 1 yield $N_i = 8.0$ and 8.7 for the circular and square cross sections. Since the number of turns before intersecting the wall is fairly large, the helix should be equivalent to a worm-like chain in a pore of width $D_{\rm eff} = D - 2r_0$. To check the equivalence quantitatively, we use Eq. (21) with $D_{\rm eff} = D - 2r_0$ and the values of λ_0 in the caption of Fig. 1 to predict the amplitudes $A_\circ$, $A_\square$. This yields

$$A_\circ = 2.45 \pm 0.05 \ , \qquad A_\square = 1.12 \pm 0.04 \ , \tag{22}$$

in good agreement with the results (6) for semi-flexible polymers.

We have also studied the dependence of $D_{\rm eff}$ on the polymer pitch p_0, keeping the radius r_0 and the persistence length L_p constant. For small p_0 the polymer makes many turns before intersecting the wall and is equivalent to a semi-flexible polymer in a pore of diameter $D-2r_0$, as discussed in the preceding paragraph. In the limit $p_0 \to \infty$, the helical polymer does not make any turns before intersecting the wall and corresponds to a semi-flexible polymer in a pore of diameter D. As p_0 increases from 0 to ∞, $D_{\rm eff}$ is expected to vary monotonically between these two limiting values.

For various values of p_0 we have computed the probability $P(n)$ that a helical polymer with radius $r_0 = 0.3$, persistence length $L_p = 8000$, and contour length nds in a cylindrical pore with a circular cross section of diameter $D = 1$ does not intersect the wall. The corresponding λ_0 was obtained from an exponential fit (19) for large n. Finally $D_{\rm eff}$ was calculated using Eq. (21) and the best estimate (6) for $A_\circ$. The results are shown in Fig. 2. The data do indeed interpolate between the expected limiting values $D - 2r_0 = 0.4$ and $D = 1$ for small and large p_0, respectively.

The crossover region in Fig. 2, where $D_{\rm eff}$ varies most rapidly with p_0, is around $p_0 \approx 40$, $D_{\rm eff} \approx 0.7$. According to Eqs. (3), (4), and (20), these values of p_0 and $D_{\rm eff}$ correspond to $N_i = (\xi L_p)^{1/3} D_{\rm eff}^{2/3}/(A_\circ p_0) \approx 0.2$ turns of the helix before intersecting the wall.

VI. HELICAL POLYMER ENCIRCLING A CYLINDRICAL ROD

In this Section we consider a helical polymer wound around a long cylindrical rod with a circular cross section and diameter $D \ll L_p$. We study the possibility that the polymer generated in the simulation escapes from the rod as n increases and wanders away.

In the simulations the parameters $ds = 10^{-4}$, $b_1/k_BT = b_2/k_BT = b_3/k_BT = L_p = 8000$ were the same as in the preceding section. The diameter of the rod was $D = 0.2$, and the radius of the helix was $r_0 = 0.3$. For these parameters $ds \ll D < 2r_0 \ll L_p$. The starting point of the polymer was chosen randomly, apart from the requirements that the stress-free helix wind around the cylindrical rod without touching it, with the axis of the helix parallel to the rod.

¿From the simulation data we computed the probability $P(n)$ that after n steps the polymer has not yet intersected the rod [26]. Each curve $P(n)$ is based on $10,000$ independent helices. The results for three different values of the pitch p_0 are shown in Fig. 3. Unlike the case of a polymer in a cylindrical pore, shown in Fig. 1, $P(n)$ does not decay to zero as n increases. Instead, above a characteristic value which depends on the pitch, the curve flattens and approaches a nonzero limiting value. This is because the polymer generated in the simulation sometimes escapes from the rod, due to a sufficiently large fluctuation, and wanders away as n increases, without ever returning to intersect the rod.

A simple theory of the escape, which suggests $P(n) = A + Be^{-Cn}$, in qualitative consistency with Fig. 3, is given in the Appendix.

We determined the average number of turns at which the helix escapes from the rod or intersects it by making two checks after each step of the growth algorithm: (i) If the distance of the endpoint $\mathbf{r}(s)$ from the axis of the rod is less than $D/2$, the polymer has intersected the rod. (ii) If the distance of the endpoint $\mathbf{r}_{\rm axis}(s)$ of the *axis* of the helix is greater than $r_0 + D/2$, the circular cross section of the helix no longer encircles the rod, i.e. the helix has escaped. Geometrically $\mathbf{r}_{\rm axis}(s)$ is determined as follows: Since the unit vectors $\mathbf{t}_3(s)$ and $\mathbf{e}(s)$ are tangent to the helix and directed along its axis, respectively, $\mathbf{e}(s) \times \mathbf{t}_3(s)$ is

directed perpendicularly from the point $\mathbf{r}(s)$ on the helix contour toward the corresponding point $\mathbf{r}_{\rm axis}(s)$ on the axis of the helix. Thus,

$$\begin{aligned}\mathbf{r}_{\rm axis}(s) &= \mathbf{r}(s) + r_0 \frac{\mathbf{e}(s)\times\mathbf{t}_3(s)}{|\mathbf{e}(s)\times\mathbf{t}_3(s)|} \\ &= \mathbf{r}(s) + \mathbf{t}_1(s)\frac{\omega_{02}}{\omega_0^2} - \mathbf{t}_2(s)\frac{\omega_{01}}{\omega_0^2}\ , \end{aligned} \tag{23}$$

where we have used Eqs. (12) and (13).

In Fig. 4 the average numbers of turns N_e^1, N_e^2 at which the helix escapes from the rod and the average number of turns N_i at which the helix intersects the rod are shown as functions of p_0. For each value of p_0, 10,000 independent configurations were generated. Each configuration was continued until it intersected the rod [26] or the number of steps of the algorithm exceeded 5×10^6, whichever came first. The average N_e^1 is based on all configurations which escape, independent of whether they return to intersect the rod or not. The quantity N_e^2 is the average value for only those configurations which escape and in 5×10^6 steps of the algorithm still have not intersected the rod.

For $p_0 \le 1$ the probability of the polymer escaping from the rod is so small that $N_e^{1,2}$ could not be determined reliably with configurations of 5×10^6 steps. For larger p_0, the data for N_e^1 and N_e^2 practically coincide, indicating that the polymer rarely returns to intersect the cylinder once it has escaped. The data are in excellent agreement with $N_e^{1,2}, N_i \sim p_0^{-1}$ for large p_0 and $N_i \sim p_0^{-2/3}$ for small p_0. These power laws may be understood as follows.

The transverse fluctuations of the endpoint of the axis of an *unconfined* helical polymer of length ℓ and persistence length P about the corresponding endpoint of the unstressed helix are readily calculated from Eq. (16) and given by [27]

$$\langle r_\perp^2\rangle = \frac{2}{3}\,\frac{\ell^3}{P} \tag{24}$$

for $\ell \ll P$. Here both $\ell = \xi s$ and $P = \xi L_p$ are measured along the axis of the helix, as discussed below Eq. (20). Equation (24) also applies to the worm-like chain. Apart from the factor 2/3, Eq. (24) follows from simple scaling or dimensional arguments [18, 19, 20]. The powers of $r_\perp$, ℓ, and P in Eq. (24) are also consistent with $E_0\ell \sim 1$ and $r_\perp \sim D$ in Eqs. (3) and (4).

Replacing $r_\perp$ in Eq. (24) by $r_0 + D/2 = 0.4$, as in the simulations, and solving for $N_e = \ell/p_0$ yields the estimate

$$N_e = \frac{12}{p_0^{2/3}\left(p_0^2+3.6\right)^{1/6}}\ . \tag{25}$$

for the number of turns of the helix at which the typical transverse displacement equals the value needed for escape from the rod. Roughly speaking, the polymer wrapped around the rod escapes in N_e turns, as given by Eq. (25) for $N_e \lesssim 1$, i.e. $p_0 \gtrsim 12$. For smaller p_0, the typical transverse fluctuations in a single turn of the helix are too small for escape from the rod, and the helix is more likely to intersect the rod than to escape. Equation (25), which ignores this possibility, no longer applies. As noted above, for $p_0 < 1$ the escape probability is too small for a reliable determination of $N_e^{1,2}$ with configurations of 5×10^6 steps.

In the region $N_e \lesssim 1$, i.e. $p_0 \gtrsim 12$, Eq. (25), which corresponds to the solid curve in Fig. 4, is in good quantitative agreement with the simulation data for $N_e^{1,2}$. For large p_0, $N_e \approx 12/p_0$. The coefficient 12 is an order-of-magnitude estimate that happens to give a good fit to the simulation data, whereas the power law $N_e \sim p_0^{-1}$ for large p_0 is exact. An argument based on Eq. (24) similar to the one for N_e predicts $N_i \sim p_0^{-1}$ for large p_0, in excellent agreement with Fig. 4. Note that the data points for $N_e^{1,2}$ and N_i practically coincide.

Since the possibility of escape is negligible for small p_0, the helical polymer is equivalent to a worm-like chain in a pore with diameter $D_{\rm eff} = 2r_0 - D$. To estimate the average number of turns N_i at which the polymer intersects the rod, we replace D by $D_{\rm eff}$ in Eqs. (3) and (4) and solve for the typical intersection length $\ell \approx E_0^{-1}$. This yields $\ell \sim P^{1/3}$. Substituting $r_\perp \sim D_{\rm eff}$ in Eq. (24) and solving for ℓ leads to the same result. According to the discussion below Eq. (20), $P = \xi L_p \approx L_p(p_0/2\pi r_0)$ for $p_0 \ll r_0$. Keeping track of the powers of p_0, we obtain the power law $N_i = \ell/p_0 \sim p_0^{-2/3}$ for small p_0, in excellent agreement with the simulation data in Fig. 4

In Fig. 5 the fractions f_e^1, f_e^2, and f_i of the 10,000 configurations which contribute to N_e^1, N_e^2, and N_i in Fig. 4 are shown as functions of p_0. For $p_0 \lesssim 1$, $f_e^{1,2} \approx 0$ and $f_i \approx 1$, i.e. almost all the configurations intersect the cylinder and never escape. Around $p_0 \approx 10$ the curves cross, and for larger p_0 the polymer is more likely to escape than to intersect the rod.

VII. CONCLUDING REMARKS

We have studied some statistical properties of a helical polymer in cylindrical restrictive geometries of diameter D, in the limit that the persistence length P along the axis of the helix is large in comparison with D and the radius r_0 of the helix. In this limit the helical

polymer has much in common with the worm-like chain. We interpret the simulation data for the free energy of confinement in a cylindrical pore using the scaling form (4) for a worm-like chain in a pore, with an effective diameter $D_{\rm eff}$ that is renormalized by the helical structure. As the pitch p_0 of the helix increases from 0 to ∞, $D_{\rm eff}$ increases monotonically from $D - 2r_0$ to D, as shown in Fig. 2.

Thinking in terms of a worm-like chain also proves useful in connection with the escape of the helical polymer encircling a cylindrical rod. In the limit $P \gg r_0$ the transverse fluctuations of the axis of the helix are given by the same result (24) as for the worm-like chain. As p_0 increases, the typical transverse displacement in one turn of the helix also increases, resulting in a greater probability per turn of escape. We have used Eq. (24) to estimate the average number of turns at which the helix escapes from the rod or intersects it. The simulation data in Fig. 4 are in excellent agreement with the predicted asymptotic forms $N_e, N_i \sim p_0^{-1}$, $N_i \sim p_0^{-2/3}$ for large and small p_0, respectively.

It would be interesting to include an attractive interaction between the rod and the polymer wound around it. In the fibril formation mentioned in the Introduction, the attraction is an essential ingredient.

Acknowledgments

AL and TWB thank Gerhard Gompper and coworkers for hospitality at the Forschungszentrum Jülich. GG acknowledges the hospitality of the Aspen Center for Physics during the final stages of this work.

APPENDIX A: SIMPLE THEORY OF ESCAPE OF A POLYMER

Let us define P_N^{ne} as the probability that the polymer has neither intersected the cylindrical surface of the rod nor escaped in the first N turns of the helix and P_N^e as the probability that it has not yet intersected the cylindrical surface but that that it has escaped. Treating each turn of the helix as statistically independent, we denote the probability that a polymer which has not yet escaped does escape in the next turn by q, and the probability that it neither escapes nor intersects the rod in the next turn by p. (The third possibility, that it intersects the rod in the next turn, has probability 1-q-p.) In addition we assume that once

the polymer escapes, it never intersects the rod.

These assumptions imply the recurrence relations

$$P^{ne}_{N+1} = pP^{ne}_N \ , \tag{A1}$$

$$P^{e}_{N+1} = qP^{ne}_N + P^{e}_N \ , \tag{A2}$$

with initial conditions $P^{ne}_0 = 1$, $P^{e}_0 = 0$. Writing down the first few iterates, it is easy to see that

$$P^{ne}_N = p^N \ , \tag{A3}$$

$$P^{e}_N = q\,\frac{1-p^N}{1-p} \ . \tag{A4}$$

The probability $P_N = P^{ne}_N + P^{e}_N$ that the polymer has not yet intersected the rod after N steps is analogous to $P(n)$ in Section V. From Eqs. (A3) and (A4)

$$P_N = \frac{q}{1-p} + \frac{1-p-q}{1-p}\,p^N \ . \tag{A5}$$

Thus, as N increases, P_N decays exponentially from $P_0 = 1$ to $P_\infty = q/(1-p)$. The mean number of turns N_e at which escape occurs is given by

$$N_e = \frac{\sum_{N=1}^{\infty} N[P^{e}_N - P^{e}_{N-1}]}{\sum_{N=1}^{\infty}[P^{e}_N - P^{e}_{N-1}]} = \frac{1}{1-p} \ . \tag{A6}$$

An analogous calculation for the mean number of turns N_i at which the polymer insects the rod yields $N_i = N_e$.

This theory is obviously an oversimplification, but the form (A5) of the decay, $P_N = A + Be^{-CN}$, is qualitatively consistent with Fig. 3.

[1] D. S. Chung, G. B. Benedek, F. M. Konikoff, and J. M. Donovan, Proc. Natl. Acad. Sci. USA **90**, 11341 (1993).

[2] Y. V. Zastavker, N. Asherie, A. Lomakin, J. Pande, J. M. Donovan, J. M. Schnur, and G. B. Benedek, Proc. Natl. Acad. Sci. USA **96**, 7883 (1999).

[3] P. Yager and P. E. Schoen, Mol. Cryst. Liq. Cryst. **106**, 371 (1984).

[4] J. M. Schnur, Science **262**, 1669 (1993).

[5] B. N. Thomas, C. M. Lindemann, and N. A. Clark, Phys. Rev. E **59**, 3040 (1999).

[6] S. Pakhomov, R. P. Hammer, B. K. Mishra, and B. N. Thomas, Proc. Natl. Acad. Sci. USA **100**, 3040 (2003).

[7] S. G. Zhang, T. Holmes, C. Lockshin, and A. Rich, Proc. Natl. Acad. Sci. USA **90**, 3334 (1993).

[8] A. Aggeli, M. Bell, N. Boden, J. N. Keen, P. F. Kowles, T. C. B. McLeish, M. Pitkeathly, and S. E. Radford, Nature **386**, 259 (1997).

[9] I. A. Nyrkova, A. N. Semenov, A. Aggeli, and N. Boden, Eur. Phys. J. B **17**, 481 (2000).

[10] I. A. Nyrkova, A. N. Semenov, A. Aggeli, M. Bell, N. Boden, and T. C. B McLeish, Eur. Phys. J. B **17**, 499 (2000).

[11] R. Oda, I. Huc, M. Schmutz, S. J. Candau, and F. C. MacKintosh, Nature **399**, 566 (1999).

[12] C.-F. Chou, R. H. Austin, O. Bakajin, J. O. Tegenfeldt, J. A. Castelino, S. S. Chan, E. C. Cox, H. Craighead, N. Darnton, T. Duke, J. Han, S. Turner, Electrophoresis **21**, 81 (2000).

[13] N. Giordano and J.-T. Cheng, J. Phys.: Condens. Matter **13**, R271 (2001)

[14] R. M. Jendrejack, E. T. Dimalanta, D. C. Schwartz, M. D. Graham, and J. J. de Pablo, Phys. Rev. Lett. **91**, 038102 (2003).

[15] P.-G. de Gennes, *Scaling Concepts in Polymer Physics* (Cornell University Press, Ithaca, 1979).

[16] T. W. Burkhardt and I. Guim, Phys. Rev. E **59**, 5833 (1999).

[17] P. Sotta, J. Chem. Phys. **112**, 1565 (2000).

[18] T. Odijk, Macromolecules **16**, 1340 (1983); *ibid.* **19**, 2313 (1986).

[19] M. Dijkstra, D. Frenkel, and H. N. W. Lekkerkerker, Physica A **19**, 374 (1993).

[20] T. W. Burkhardt, J. Phys. A **30**, L167 (1997).

[21] D. J. Bicout and T. W. Burkhardt, J. Phys. A **34**, 5745 (2001).

[22] S. Panyukov and Y. Rabin, Phys. Rev. Lett. **85**, 2404 (2000).

[23] S. Panyukov and Y. Rabin, Phys. Rev. E **62**, 7135 (2000).

[24] Y. Kats, D. A. Kessler, and Y. Rabin, Phys. Rev. E **65**, 020801(R) (2002).

[25] In the absence of fluctuations Eq. (7) implies $d^2\mathbf{t}_3/ds^2 = \boldsymbol{\omega}_0 \times (\boldsymbol{\omega}_0 \times \mathbf{t}_3) = -\omega_0^2 \mathbf{t}_3 + \boldsymbol{\omega}_0 \omega_{03}$, which has the solution $\mathbf{t}_3(s) = \mathbf{A}\cos(\omega_0 s) + \mathbf{B}\sin(\omega_0 s) + \mathbf{e}(0)\omega_{03}/\omega_0$. Choosing the integration constants $\mathbf{A}$, $\mathbf{B}$ to fit the initial conditions and integrating $d\mathbf{r} = \mathbf{t}_3 ds$ yields Eq. (11).

[26] The cylindrical boundary is assumed to be an hard wall. In all but tangential intersections of the polymer with the wall, $\mathbf{t}_3 = d\mathbf{r}/ds$ must change discontinuously, to avoid penetration. However, in the model of Section II the discontinuity costs an infinite bending energy and is also forbidden. In the simulations a polymer configuration that intersects the boundary at step n of the algorithm should not be continued to larger n, since both penetration and reflection are forbidden. Tangential intersections with continuous $\mathbf{t}_1, \mathbf{t}_2, \mathbf{t}_3$ are allowed, but they represent a negligible fraction of all intersections.

[27] Equation (24) is obtained by writing $\mathbf{r}_\perp(s) = [\mathbf{I} - \mathbf{e}(0)\mathbf{e}(0)] \cdot \int_0^s \mathbf{e}(s')\xi ds'$, where $\mathbf{I}$ is the unit dyadic, calculating the second moment $\langle r_\perp^2(s) \rangle$ with the help of Eq. (16), and making use of $P = \xi L_p$, $\ell = \xi s$, as discussed below Eq. (20).

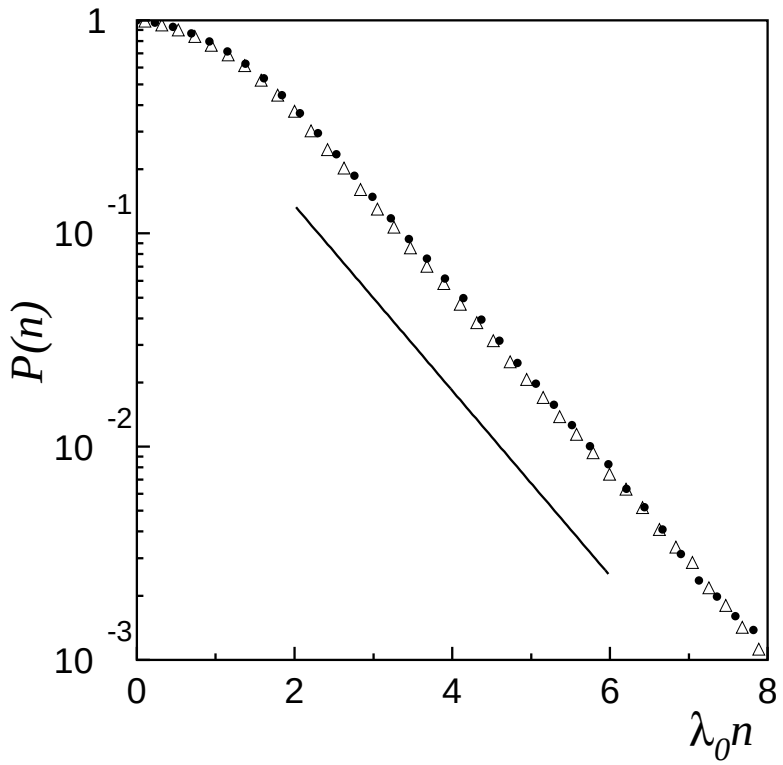

FIG. 1: Probability $P(n)$ that a helical polymer with radius $r_0 = 0.3$, pitch $p_0 = 0.3$, and persistence length $L_p = 8000$ in a cylindrical pore does not intersect the pore wall in the first n steps of the algorithm. The full circles (•) correspond to a pore with a circular cross section with diameter $D = 1$ and the triangles (△) to a square cross section with edge length $D = 1$. Fitting the data to Eq. (19) for large n yields $\lambda_0 = 6.57 \times 10^{-6}$ and 6.01×10^{-6}, respectively. The full line corresponds to the exact exponential decay $e^{-\lambda_0 n}$.

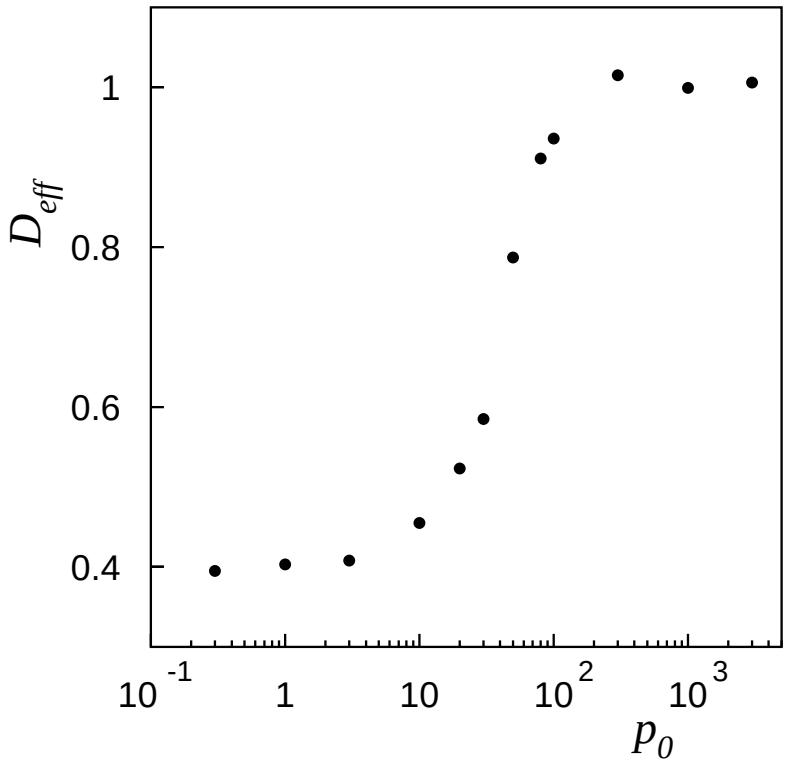

FIG. 2: The effective diameter D_{eff} as a function of the pitch p_0 for a helical polymer with radius $r_0 = 0.3$ and persistence length $L_p = 8000$ in a cylindrical pore with a circular cross section with diameter $D = 1$. The data interpolate between the limiting values $D - 2r_0 = 0.4$ and $D = 1$ for small and large p_0, respectively.

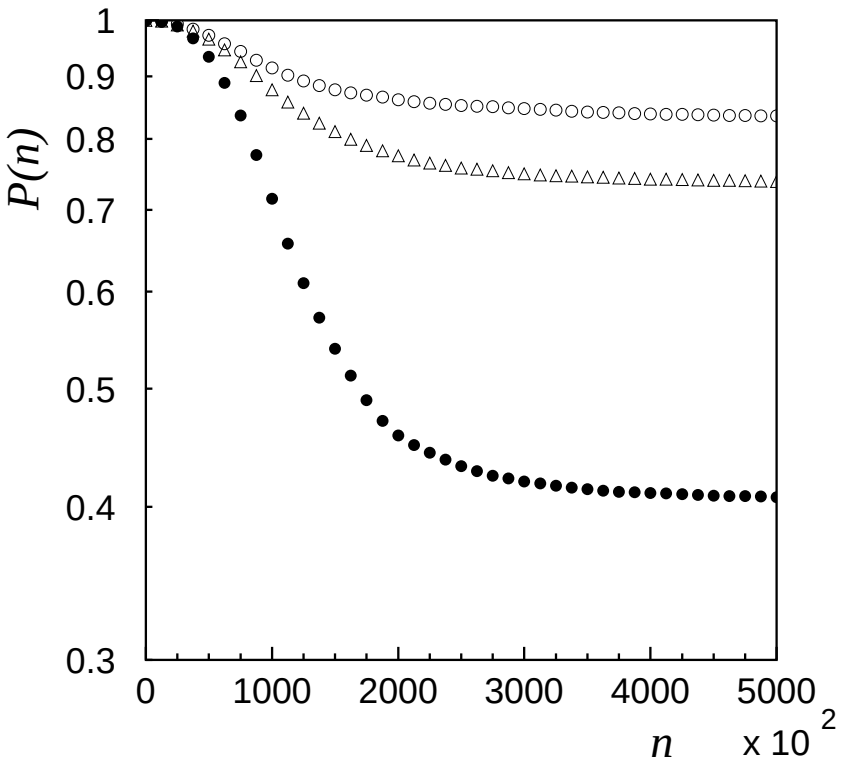

FIG. 3: Probability $P(n)$ that a helical polymer with radius $r_0 = 0.3$ and persistence length $L_p = 8000$, wound at the fixed end around a cylindrical rod of diameter $D = 0.2$ does not intersect the rod in the first n steps of the algorithm. The pitch of the helix is $p_0 = 10$ (•), 30 (△), and 100 (○).

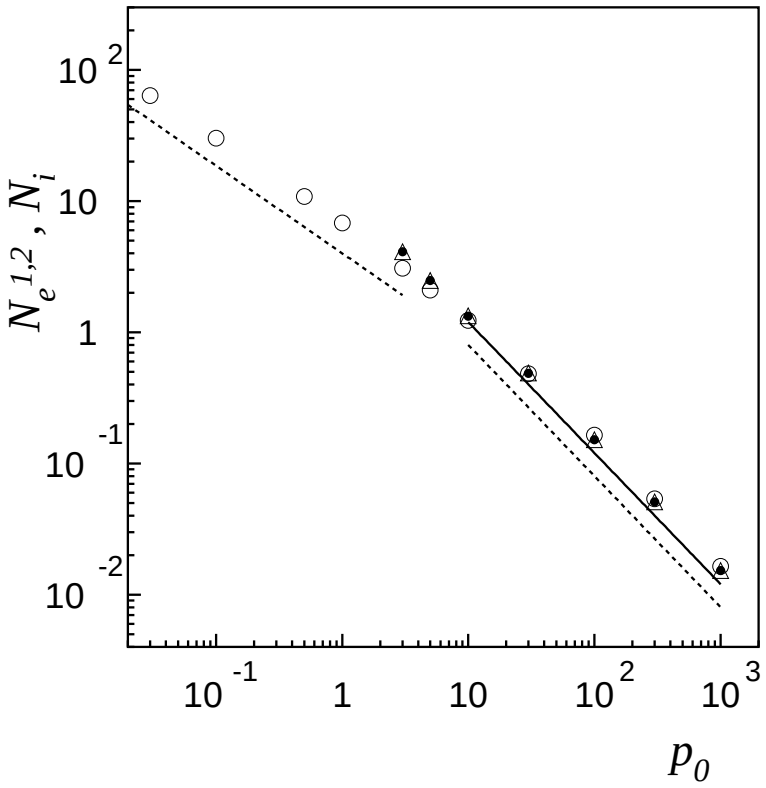

FIG. 4: Average numbers of turns N_e^1 ($\triangle$), N_e^2 ($\bullet$) at which the helix escapes from the rod, and the average number of turns N_i ($\circ$) at which the helix intersects the rod as a function of p_0. Here N_e^1 is based on all the configurations which escape, independent of whether they return to intersect the rod or not; N_e^2 is based on the configurations which escape and in 5×10^6 steps of the algorithm do not return to intersect the rod. The dashed lines on the left and right have slopes -2/3 and -1, respectively, and the solid line shows the prediction (25).

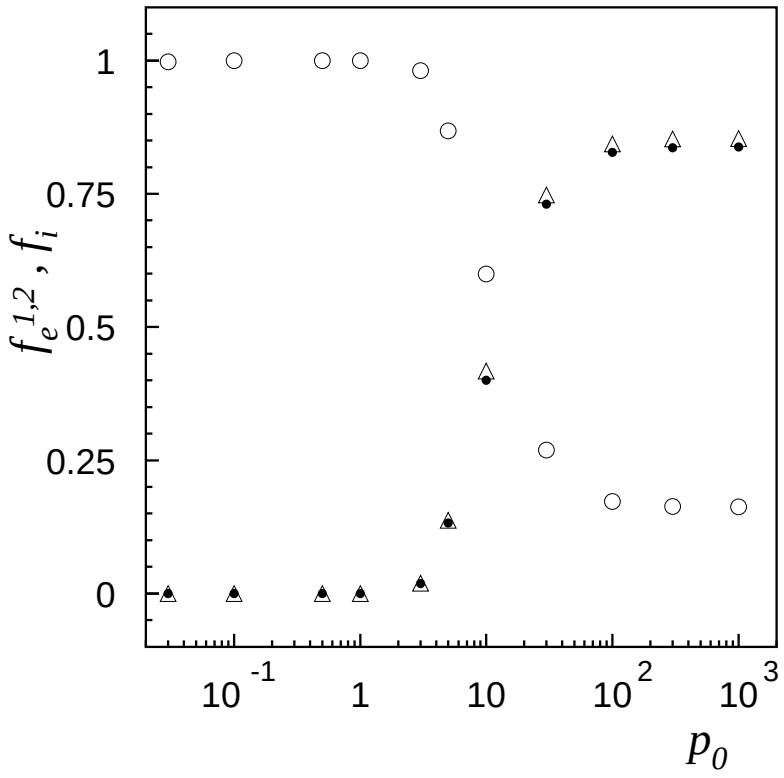

FIG. 5: Fractions f_e^1 (△), f_e^2 (•), and f_i (○) of the 10,000 configurations which contribute to N_e^1, N_e^2, and N_i in Fig. 4, as a function of p_0.